Density Functional Theory Investigation of EPR Parameters for Tetragonal Cu(II) Model Complexes with Oxygen Ligands†

William M. Ames and Sarah C. Larsen*

Department of Chemistry, The University of Iowa, Iowa City, Iowa 52242

Received: December 11, 2008; Revised Manuscript Received: February 18, 2009

Density functional theory (DFT) calculations of the electron paramagnetic resonance (EPR) parameters for a series of tetragonal Cu(II) model complexes were conducted. Model complexes containing four oxygen atoms directly coordinated to a Cu(II) metal center were chosen because of their importance in the Peisach−Blumberg truth tables and their frequent use in the interpretation of EPR spectra of Cu(II) proteins and copper-containing catalysts. Molecular **g**- and copper **A**-tensors were calculated using the BP86 and B3LYP density functionals. The DFT calculations reproduce the experimentally observed trends in the parallel components of the **A**- and **g**-tensors. Important insight into the structural basis for the empirical trends in $g_{||}$ and $A_{||}$ was obtained from the DFT calculations. Notably, $g_{||}$ systematically increases and $A_{||}$ systematically decreases with increasing Cu−O equatorial bond length. These results have been used to provide structural insight into copper EPR data for copper-exchanged zeolites.

I. Introduction

Electron paramagnetic resonance (EPR) is a valuable spectroscopic tool for determining the coordination environment of Cu(II) complexes. Divalent copper has a d^9 electronic configuration with one unpaired electron and a nuclear spin of 3/2. The **g**- and copper **A**-tensors are strongly influenced by the ligand environment of the Cu(II) atom. When the copper atom is coordinated to an atom with a nuclear magnetic moment greater than zero, ligand-hyperfine splittings can sometimes be observed, providing a direct way to determine the ligand environment around a Cu(II) metal center. In the absence of resolved ligand hyperfine splittings, the copper **g** and **A** values can be used in conjunction with model complex data to interpret the EPR spectra for copper (II) complexes.

Peisach and Blumberg developed empirical correlations between the parallel components of **g** and **A**, the $g_{||}$ and copper $A_{||}$ parameters, respectively, for tetragonal Cu(II) complexes in specific ligand coordination environments.[1] These EPR "truth tables" for tetragonal Cu(II) complexes have been used extensively to interpret the EPR spectra of Cu(II) protein complexes and many other novel Cu(II) complexes. Each "truth table" indicates an experimentally observed correlation between $g_{||}$ and copper $A_{||}$ with the overall charge of the complex in a specific ligand coordination environment.

In recent years, computational chemistry has become an increasingly important research tool. Methods based in quantum mechanics (QM) can provide information about relative energies, reaction coordinates, vibrational energies, and molecular geometries. The use of QM methods, such as Hartree−Fock (HF), post HF, and density functional theory (DFT), provides a synergy between experiment and theory and has become significantly more popular as availability of increasingly powerful personal computers has made computational chemistry more accessible. QM methods have, in recent years, proven to be valuable resources for calculating EPR parameters and correlating proposed structures with experimental EPR results.[2−14] Methods utilizing DFT have been developed to calculate EPR parameters of organic radicals and EPR active transition metal complexes.[15−19] While the ultimate goal is to use DFT calculations to provide quantitative agreement with experiment, there are many examples where reproducing an experimentally observed trend using DFT calculations can provide significant structural insight, even if the quantitative agreement between experiment and theory is not optimal.[20−24]

The calculation of EPR parameters for transition metal complexes using DFT remains a challenge although significant progress has been made. For EPR active transition metal systems, the density functional chosen for the EPR parameter calculations has proven to be particularly important. With current methodologies, hybrid density functionals provide the best overall performance when compared to generalized gradient, GGA, functionals for the calculation of EPR parameters.[25−29] More recently, the application of meta-GGA[30] and double hybrid density functionals[31] have shown promise in the calculation of hyperfine coupling constants of transition metal complexes.[32] Additionally the spin−orbit coupling, SOC, effects for transition metal complexes on EPR parameters can be quite large; the improvements gained through the application of appropriate SOC operators on calculated **g**- and **A**-tensors have been previously reported.[25,33] These methods for calculating EPR parameters with DFT have been incorporated into a number of readily available commercial and academic software packages.

Previous studies of DFT methods applied to the EPR parameters of copper complexes have been reported. Larsen and Saladino reported DFT EPR parameter calculations for the $Cu(acac)_2$ and $[Cu(ox)_2]^{2-}$ complexes incorporating scalar relativistic and SOC effects.[34] Neese has investigated the applicability of DFT methods for calculating the EPR parameters of a number of copper complexes, including the $Cu(acac)_2$ complex.[25−27] Recently Almeida and co-workers reported calculations of EPR parameters using DFT methods for Cu(II) aqua complexes.[14] The limitations of DFT methods with respect to the accurate calculation of EPR parameters for copper complexes have been explored in these previous studies and have motivated the

† Part of the "George C. Festschrift".

* To whom correspondence should be addressed. E-mail: sarah-larsen@uiowa.edu.

10.1021/jp810924j CCC: $40.75
Published on Web 03/16/2009

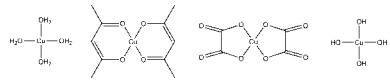

Figure 1. Basic model complexes studied: $[Cu(H_2O)_4]^{2+}$; $Cu(acac)_2$; $[Cu(ox)_2]^{2-}$; $[Cu(OH)_4]^{2-}$.

present study in which trends in EPR parameters for copper model complexes will be investigated. Since the DFT calculations systematically deviate from the experimental EPR parameters for structurally similar copper complexes, structural insight can be obtained when evaluating trends in EPR parameters.

In the study reported here, DFT methods are used to calculate the EPR parameters for Cu(II) complexes containing a ligand environment of four oxygen atoms strongly coordinated to the copper metal center in a square planar arrangement. The objective of this study is to reproduce the observed trend in $g_{||}$ and $A_{||}$ and to provide structural insight into this empirical trend for copper model complexes. The series of complexes investigated in this study were selected from the Peisach−Blumberg truth tables and are shown in Figure 1. The model complexes include the hydrated Cu(II) complex under high, $[Cu(OH)_4]^{2-}$, and low pH conditions, $[Cu(H_2O)_4]^{2+}$, copper acetylacetonate, $Cu(acac)_2$, and copper oxalate anion, $[Cu(ox)_2]^{2-}$ complexes. The results of this study were used to provide additional structural insight into previously obtained EPR data for copper-exchanged zeolites.

II.Computational Details

Geometry Optimization. The geometries of the copper complexes were optimized using the ORCA program package.[35] Each structure was optimized with no constraints using a modified version of the "Accurate Optimization" procedure built into ORCA with the unrestricted Kohn−Sham (UKS) formalism. This consisted of replacing the default density functional and basis sets used for the optimization. For this study, the B3LYP functional was used in place of the BP86 functional and the basis set Default Basis 5 (DB5) replaced the Default Basis 4 (DB4) normally used with the Accurate Optimization feature. The B3LYP functional contains 20% Hartree−Fock (HF) exchange with 72 and 81% scaling of the generalized gradient approximation (GGA) Becke exchange[36] and Lee−Yang−Parr correlation,[37] respectively. In addition, B3LYP utilizes the VWN-5 parametrized electron gas data of Vosko et al. for the local correlation.[38] DB4 consists of a triple-ζ basis set on all atoms with a single polarization function for the hydrogen atoms and two sets of polarization functions for all other atoms.[39] DB5 differs from DB4 in that diffuse functions are added to all atoms, including hydrogens. The resolution of the identity (RI) approximation[40,41] was used during the geometry optimizations with the RIJONX flag to speed up the self-consistent field (SCF) convergence during each optimization step. The auxiliary basis sets used with the RI approximation are built automatically by ORCA.

The optimizations of the $Cu(acac)_2$ and $[Cu(ox)_2]^{2-}$ complexes were compared with previously published X-ray crystal structures,[42,43] and no significant deviations were observed. It has been assumed that the structures for the remaining complexes are of acceptable quality to provide reasonable results for the calculation of EPR parameters.

EPR Parameter Calculations. The ORCA program package was used to calculate the **g**- and **A**-tensors of the copper transition metal center for each model complex. The methods for calculation of the **g**- and **A**-tensors were developed and implemented into the ORCA program by Neese.[25,26,33] The **A**-tensor is calculated as a sum of three terms: (a) the isotropic Fermi contact term, (b) the spin-dipolar term, and (c) the spin−orbit coupling term. To produce a good estimation for the Fermi contact, calculations need to include appropriate spin-polarization, which can be achieved through the use of the UKS formalism.

Two different exchange and correlation functional combinations have been used to calculate the EPR parameters: the GGA BP86 functional and the B3LYP hybrid density functional. The BP86 functional was chosen due to its popularity, and the B3LYP functional was used because of previous success when calculating EPR parameters for transition metal complexes.[25−27,29] The BP86 functional uses the parametrized electron gas data from Perdew and Wang[44] as the local density approximation (LDA) implementation and the Becke gradient correction[36] for exchange along with the correlation correction of Perdew.[45]

The basis sets used for the EPR parameter calculations were the core properties (CP) basis set, developed by Neese,[46] with three polarization functions for the copper transition metal center and the DB4 basis set for all other atoms. The CP basis set contains additional steep primitives at the core region, improving calculated core property values, such as the **A**-tensor. The RI approximation was used for both functionals to speed up calculations of the EPR parameters. Auxiliary basis sets for use with the RI approximation were constructed automatically by ORCA.

Calculations of the EPR parameters utilized the complete mean-field spin-orbit (SO) operator for the Coulomb term. The RI approximation was utilized with the SO operator to reduce computation times. The convergence tolerances and integration accuracies of the calculations were increased from the defaults using the available TightSCF and Grid5 options. Additionally the integration accuracy around the copper atom was increased to 9.000, which gives better results for calculations of the hyperfine coupling constants of the Cu(II) metal center.

Comparison with Experimental Parameters. Copper complexes with readily available and previously published experimental EPR data were chosen for this study. Despite careful construction of our models some issues with comparing our calculated EPR parameters with experimentally derived EPR parameters need to be considered. The experimental EPR parameters were measured using EPR spectroscopy and as such can only determine the absolute values of the EPR hyperfine parameters. To facilitate the comparison of our calculated copper **A**-tensors with the experimentally determined **A** values, the absolute values of our calculated values are compared to those from experiment. A point of additional concern lies in the fact that our calculations are done in vacuo, ignoring environmental effects. It has been assumed that solvent/environmental effects should be largely systematic for the EPR parameters and models investigated. Additionally the perturbation due to the environment is often assumed to represent a small percentage of the error in EPR parameter calculations with the majority of the error occurring due to limitations inherent in current computational methodologies. The effect of these assumptions on the calculated parameters will be discussed in later sections.

III. Results and Discussion

Model Complex Geometries. For divalent copper complexes the coordination environment is generally distinguished by four strongly coordinated atoms occupying a square planar arrangement. Often one or two additional atoms are weakly coordinated in axial positions, perpendicular to the plane defined by the strongly coordinated atoms, giving a distorted octahedral or

TABLE 1: Optimized Geometries for Model Complexes used in EPR Parameter Calculations

		bond lengths (Å)			
		calculated		experimental	
complex	geometry	Cu−O	Cu−L[a]	Cu−O	Cu−L[a]
$[Cu(H_2O)_4]^{2+}$	square planar	1.947/1.997			
$[Cu(H_2O)_5]^{2+}$	square pyramidal	1.984/2.025	2.193	1.96[b]	2.36[b]
		1.975/1.995[c]	2.162[c]		
$[Cu(H_2O)_6]^{2+}$	octahedral	2.018/2.032	2.305	2.01[d], 1.95[e]	2.33[d], 2.29[e]
		1.998/2.001[c]	2.255[c]		
$[Cu(OH)_4]^{2-}$	square planar	1.840			
$[Cu(ox)_2]^{2-}$	square planar	1.959		1.929/1.930[f]	
$Na_2Cu(ox)_2$	square planar	1.955			
$Na_2Cu(ox)_2H_2O$	square pyramidal	1.977/1.961	2.508		2.803[f,g]
$Cu(acac)_2$	square planar	1.940		1.912/1.914[h]	
$Cu(acac)_2THF$	square pyramidal	1.952/1.961	2.503		
$Cu(acac)_2THF_2$	octahedral	1.963	2.663		
$Cu(acac)_2Py$	square pyramidal	1.967	2.397		
$Cu(acac)_2Py_2$	octahedral	1.981	2.579		

[a] The bond length of the axial ligand L with copper. [b] EXAFS results from ref 57. [c] B3LYP optimized structures of Almeida et al., see ref 14. [d] XRD measurement from ref 47. [e] EXAFS results from ref 48. [f] XRD measurement from ref 43. [g] Structure indicates axial coordination to neighboring oxalate anion in crystal, not H_2O. See ref 43. [h] XRD measurement from ref 42.

square pyramidal arrangement. These weakly coordinated atoms are generally understood to have a small impact on the EPR spectrum of a copper complex.

Selected values for bond angles and bond lengths have been included in Table 1 for the complexes investigated here. In Table 1, the number and type of axial ligands have been specified along with relevant geometric parameters. Only complexes that have been used for EPR parameter calculations are shown in Table 1; complexes that did not optimize to an appropriate square planar, square pyramidal, or octahedral geometry have not been included. A general trend can be observed where the addition of axial ligands leads to an increase in the Cu−O bond lengths of the equatorial ligands. The effect of the change in geometry on the calculated EPR parameters is discussed further in later sections.

To study the effect of axially coordinated ligands on the calculated EPR parameters in more detail, attempts were made to optimize the hydrated water complexes starting with octahedral, square pyramidal, and square planar geometries. It was found that the hydrated copper complexes at low pH ($[Cu(H_2O)_x]^{2+}$ where $x = 4$, 5, or 6) readily optimized to octahedral, square pyramidal, and square planar geometries while the complexes at high pH ($[Cu(OH)_4(H_2O)_y]^{2-}$ where $y =$ 1 or 2) would only optimize to a square planar configuration. The Cu−L bond lengths for the optimized complexes are listed in Table 1. The geometries for the square pyramidal and octahedral complexes agree well with previous results obtained by Almeida and co-workers with the B3LYP density functional.[14] Additionally for the octahedral complex, the calculated geometry presented here agrees well with experimentally determined bond lengths.[47,48]

The optimized geometries of the $Cu(acac)_2$ and $[Cu(ox)_2]^{2-}$ complexes were compared to previously published crystal structure data.[42,43] The geometry optimized structure for the $Cu(acac)_2$ complex agrees with the experimental crystal structure very well with maximum errors of ±0.03 Å and ±1.5° for bond lengths and bond angles, respectively. The optimized structure for the $[Cu(ox)_2]^{2-}$ complex has maximum errors of ±0.03 Å and ±2.0° for bond lengths and bond angles, respectively. The crystal structure of the copper oxalate complex also indicates a slight out of plane distortion due to crystal packing effects of 4.7°, which is not replicated in the optimized geometry.

The initial models of both $Cu(acac)_2$ and $[Cu(ox)_2]^{2-}$ ignore coordination due to solvent molecules in an axial position to the Cu(II) metal center. To address this issue and investigate the effects of axial ligand coordination, larger model complexes of the $Cu(acac)_2$ and $[Cu(ox)_2]^{2-}$ were constructed and optimized. Square pyramidal, $x = 1$, and octahedral, $x = 2$, geometries of the $Cu(acac)_2L_x$ complex were optimized where the axial ligand, L, was either tetrahydrofuran, THF, or pyridine, Py. Additionally, the $[Cu(ox)_2(H_2O)_x]^{2-}$ and $Na_2Cu(ox)_2(H_2O)_x$ complexes were investigated as extensions of the basic Cu(II) oxalate model with $x = 0$, 1 or 2 for square planar, square pyramidal, and octahedral geometries, respectively. The addition of Na^+ cations to the Cu(II) oxalate model was prompted by the existence of monovalent counterions in the crystal structure. With the methods and models used here, complexes containing two water molecules, $Na_2Cu(ox)_2(H_2O)_2$ and $[Cu(ox)_2(H_2O)_2]^{2-}$, did not optimize to a final octahedral geometry and the $[Cu(ox)_2(H_2O)]^{2-}$ complex failed to optimize to a final square pyramidal geometry. The final geometries for these three complexes have water molecules hydrogen bonded to the directly coordinated oxygen atoms of the oxalate anion ligands. The remaining complexes, $Na_2Cu(ox)_2$ and $Na_2Cu(ox)_2(H_2O)$ have been used for subsequent EPR parameter calculations while the $[Cu(ox)_2(H_2O)]^{2-}$, $Na_2Cu(ox)_2(H_2O)_2$ and $[Cu(ox)_2(H_2O)_2]^{2-}$ complexes were removed from consideration for further calculations in this study.

Calculated EPR Parameters for Copper Aqua Model Complexes. The hydrated Cu(II) complex at low pH has been optimized to three different structural forms, square planar, square pyramidal and octahedral. The Cu–O bond lengths of the optimized complexes (Table 1) increase as the coordination changes from square planar, to square pyramidal, to octahedral. From a qualitative perspective, the bond length trend is correlated to a trend in the localization of electron density on the transition metal center. The shorter bond lengths are indicative of stronger Cu−O bonds, or a greater sharing of electron density between the copper metal center and the ligands, leading to a delocalization of electron density about Cu(II) and a concomitant increase in the copper $A_{||}$. The longer bond lengths indicate a more localized electron density distribution about Cu(II) and a relatively smaller $A_{||}$. This trend in the electron density about Cu(II) is easily observed with EPR spectroscopy as an increase in the copper $A_{||}$ value and a decrease in the $g_{||}$

TABLE 2: Calculated $g_{||}$ and $A_{||}$ Values for Hydrated Copper at Low and High pH

	$g_{||}$				$A_{||}$ (MHz)[a]			
complex	BP86	B3LYP	B(38)LYP[b]	exp	BP86	B3LYP	B(38)LYP[a]	exp
$[Cu(H_2O)_4]^{2+}$	2.185	2.247			525	548		
$[Cu(H_2O)_5]^{2+}$	2.209	2.280	2.343		477	486	496	
$[Cu(H_2O)_6]^{2+}$	2.220	2.295	2.353	2.422[c]	461	468	470	402[c]
$[Cu(OH)_4]^{2-}$	2.090	2.126		2.273[d]	526	550		582[d]

[a] The absolute value of the $A_{||}$ values are shown here to facilitate comparison with the Peisach−Blumberg tables. $A_{||}$ values are calculated as negative quantities. [b] Data from ref 14 using the reparameterized B3LYP functional of Solomon et al.[49] [c] Experimental data from ref 52. [d] Experimental data from ref 51.

value as the delocalization increases. This empirical trend is also seen in the experimental data used in the Peisach-Bumberg truth tables.[1]

The calculated values for $A_{||}$ and $g_{||}$ for the hydrated copper complexes at varying pH are listed in Table 2. The expected trend (increasing $A_{||}$ and decreasing $g_{||}$ with decreasing Cu−O bond length) is well replicated with the calculated values. Previous calculations of the **g**- and **A**-tensor values for $[Cu(H_2O)_6]^{2+}$ and $[Cu(H_2O)_5]^{2+}$ complexes show the same trend while using a similar methodology for calculating the EPR parameters.[14,49] The values shown in Table 2 indicate that the incorporation of axial ligands can have a significant impact on calculated EPR parameters. The formation of the weak axial Cu−ligand bond perturbs the electron configuration of the complex that leads to weaker equatorial ligand bonds. The redistribution of electron density in the equatorial ligand plane as a consequence of the change in geometry leads to a noticeable shift in both the **g**- and copper **A**-tensor values. Because of the significant differences in the calculated EPR parameters between the $[Cu(H_2O)_6]^{2+}$ and $[Cu(H_2O)_4]^{2+}$ complexes, the $[Cu(H_2O)_6]^{2+}$ complex will be used to construct a truth table using DFT calculated values since it is most likely a closer representation of the complex measured experimentally in a solvent environment.

Environmental/Solvent Effects on $[Cu(ox)_2]^{2-}$. The crystal structure of the $[Cu(ox)_2]^{2-}$ complex indicates that there are counterions, Na^+ or K^+, located at the terminal ends of each oxalate, balancing the overall charge. The positions of these counterions should lead to a redistribution of electron density about the molecule resulting in a localization of density near Cu(II). Additionally, the crystal structure indicates that Cu(II) is in a distorted octahedral environment with oxygen atoms from neighboring oxalate groups axially coordinated. In a dilute solvent environment, it is likely that any axial coordination that occurs will be due to the solvent, such as water, and not nearby oxalate oxygen atoms. From the evidence provided by the calculations of EPR parameters for $[Cu(H_2O)_x]^{2+}$ complexes, the addition of axially coordinated water molecules should lead to a localization of electron density near Cu(II).

The calculated EPR parameters for each copper oxalate complex are shown in Table 3. As was anticipated based on previous results, the expected increase in the $g_{||}$ value due to the extension of the basic $[Cu(ox)_2]^{2-}$ complex with Na^+ and subsequently H_2O is observed with the calculated values. For the calculated $A_{||}$ values, the addition of Na^+ to the complex leads to a slight increase in $A_{||}$, which is consistent with the slight decrease in the Cu−O bond length (Table 1). With the subsequent addition of an axial water molecule to the complex, Cu−O bond length increases and the expected decrease in the $A_{||}$ value is observed.

Solvent Effects on $Cu(acac)_2$. Experimental evidence suggests that the solvent plays a significant role in the experimental **g**- and copper **A**-tensors for the $Cu(acac)_2$ complex.[50] The effect of solvent on the experimental **g** and copper **A** values is shown in Table 4. Experiment shows that the $Cu(acac)_2$ complex in different solvents has $g_{||}$ and copper $A_{||}$ values ranging from 2.260 to 2.304 and 480 to 588 MHz, respectively, depending on the solvent. To investigate in more detail how axial ligand binding affects the $g_{||}$ and $A_{||}$ gas phase calculated values, axial coordination with pyridine and THF to $Cu(acac)_2$ was investigated.

The square pyramidal and octahedral complexes of the $Cu(acac)_2$ complex with axially coordinated THF or pyridine were optimized and EPR parameters calculated in the same manner as for all of the model complexes in this study. Selected bond lengths for each complex are shown in Table 1. The $Cu(acac)_2$ complexes axially coordinated to THF exhibit an out of plane distortion of the acac groups due to steric interference from the THF groups of 8.3 and 10.9° for the octahedral and square planar complexes, respectively. Additionally the square pyramidal pyridine complex is distorted with the two acetylacetonate groups forming an angle of 15.8° between them facing away from the axial pyridine. The octahedral complex with axial

TABLE 3: Calculated $g_{||}$ and $A_{||}$ Values for Copper Oxalate Complexes

	$g_{||}$			$A_{||}$ (MHz)[a]		
complex	BP86	B3LYP	exp	BP86	B3LYP	exp
$[Cu(ox)_2]^{2-}$	2.108	2.162	2.318[b]	516	615	492[b]
$Na_2Cu(ox)_2$	2.114	2.169		529	616	
$Na_2Cu(ox)_2H_2O$	2.123	2.183		509	588	

[a] The absolute value of the $A_{||}$ values are shown here to facilitate comparison with the Peisach−Blumberg tables. $A_{||}$ values are calculated as negative quantities. [b] Experimental data from ref 52.

TABLE 4: Experimental and Calculated Effects of Solvent on the $g_{||}$ and $A_{||}$ Values of the $Cu(acac)_2$ Complex

solvent[c]	geometry	functional	$g_{||}$	$A_{||}$[a,b]
gas phase	square planar	BP86	2.112	512
		B3LYP	2.167	604
pyridine	square pyramidal	BP86	2.127	475
		B3LYP	2.190	554
	octahedral	BP86	2.135	469
		B3LYP	2.201	542
		exp	2.274	492
tetrahydrofurane	square pyramidal	BP86	2.122	493
		B3LYP	2.181	577
	ocathedral	BP86	2.127	487
		B3LYP	2.189	567
		exp	2.278	527
piperidine		exp	2.260	515
dimethylsulfoxide		exp	2.304	480
N,*N*-dimethylformamide		exp	2.291	556
N,*N*-dimethylacetamide		exp	2.295	547
1,2-propanediol carbonate		exp	2.278	588
chloroform		exp	2.285	523

[a] Values in MHz. [b] The absolute value of the *A* values are shown here to facilitate comparison with the Peisach−Blumberg tables. *A* values are calculated as negative quantities. [c] Experimental data from ref 50.

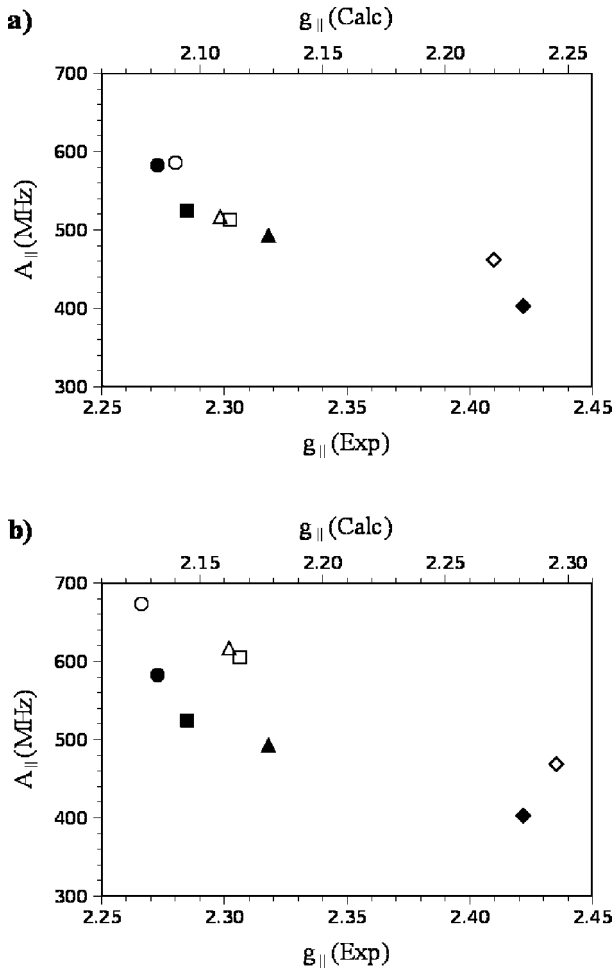

Figure 2. Plots of $g_{||}$ vs $A_{||}$ for the (a) BP86 functional and (b) the B3LYP hybrid density functional. The solid symbols are the experimentally determined values[50−52] for each complex while the open symbols are the calculated values. The diamond, triangle, square, and circle symbols are values for the $[Cu(H_2O)_6]^{2+}$, $[Cu(ox)_2]^{2-}$, $Cu(acac)_2$, and $[Cu(OH)_4]^{2-}$ complexes, respectively.

pyridine molecules only contains the usual Jahn−Teller axial distortion commonly observed with Cu(II) complexes. A general trend is observed with the Cu−O(acac) bond lengths increasing as the geometry changes from square planar to octahedral which is analogous to the trend observed for copper aqua complexes.

The results of the EPR parameter calculations for the $Cu(acac)_2$ complexes are listed in Table 4. The calculated EPR parameters show an increase in $g_{||}$ and a decrease in $A_{||}$ when the coordination of the model complex is changed from square planar to square pyramidal to octahedral. This reflects the general trend in EPR parameters with bond lengths observed for copper aqua and oxalate complexes.

Correlation Between $g_{||}$ and $A_{||}$ Calculated by DFT. The calculated and experimental $g_{||}$ and copper $A_{||}$ values for the model complexes are plotted in Figure 2 to facilitate a comparison with the original truth tables of Peisach and Blumberg.[1] The solid symbols represent the experimental EPR parameters[50−52] and the open symbols represent the calculated EPR parameters for the model complexes. The $g_{||}$ and copper $A_{||}$ values calculated using the BP86 and B3LYP density functionals are shown in Figure 2a,b, respectively. Overall, the experimentally observed trend of increasing $g_{||}$ and decreasing copper $A_{||}$ as the model complex is varied from $[Cu(H_2O)_6]^{2+}$ to $[Cu(OH)_4]^{2-}$ is reproduced in the DFT calculated values. This is the first time that this trend in EPR parameters has been reproduced using DFT calculations and suggests that the DFT calculations can provide structural insight regarding the observed trends that have been so widely used for interpreting experimental EPR data for copper proteins. However, there are some differences between the calculated and the experimental EPR parameters. When comparing the calculated data points to the experimental data points for $Cu(acac)_2$ and $[Cu(ox)_2]^{2-}$ complexes, the complexes are closer together and reversed relative to one another and this will be discussed in more detail below.

The quantitative agreement between the experimental and calculated $g_{||}$ and copper $A_{||}$ values remains a challenge. The values calculated with the GGA functional, Figure 2a, underestimate the experimental g-shift of $g_{||}$ from the electronic g value, g_e. In addition, the $g_{||}$ value range for calculated values using the BP86 functional is approximately 87% of the full experimental $g_{||}$ value range. The calculated $A_{||}$ values using the BP86 functional are generally in good agreement with the experimental values with the exception being the $[Cu(H_2O)_6]^{2+}$ complex, which is approximately 60 MHz too large.

The EPR parameter values calculated using the B3LYP hybrid density functional are shown in Figure 2b. All of the copper $A_{||}$ values calculated using the hybrid functional are overestimated. The overestimation of the $A_{||}$ values when using the B3LYP density functional is most likely due to the addition of HF exchange, which has been shown to increase calculated **g**- and transition metal **A**-tensors.[25−27,29] The $g_{||}$ values calculated using the B3LYP functional underestimate the $g_{||}$ values for all the model complexes in the original Peisach−Blumberg plots. Additionally, like the GGA functional the hybrid functional does not replicate the experimental range for the $g_{||}$ values and spans approximately 113% of the full experimental range. Qualitatively, the B3LYP hybrid functional replicates the EPR parameter trend of increasing $g_{||}$ and decreasing $A_{||}$ when varying the complex from $[Cu(H_2O)_6]^{2+}$ to $[Cu(OH)_4]^{2-}$.

The positions of the calculated EPR parameters of the $Cu(acac)_2$ and $[Cu(ox)_2]^{2-}$ complexes in Figure 2a,b are very close to each other and this is not reflected in the experimental data that shows a much greater separation of these two complexes on the graph. Both the $Cu(acac)_2$ and $[Cu(ox)_2]^{2-}$ complexes are sensitive to solvent and/or environmental effects as illustrated by the data in Tables 3 and 4. This may explain the deviation between the experimental and calculated values but does not explain the relative positions of the two complexes on the graph. The $[Cu(ox)_2]^{2-}$ and $Cu(acac)_2$ complexes coordinate to the Cu(II) metal center through carbonyl oxygen atoms which qualitatively indicates that the EPR parameters should be similar. The primary difference between the two complexes, aside from the overall charge, is the existence of resonance within the $Cu(acac)_2$ complex. This resonance delocalizes the electron density throughout the entire complex which in turn leads to a smaller $g_{||}$ value and a larger $A_{||}$ value for $Cu(acac)_2$ relative to $[Cu(ox)_2]^{2-}$. It can be seen by qualitative inspection of spin density plots shown in Figure 3, generated using gOpenMol,[53,54] that there is some delocalization occurring along the carbon atoms of the $Cu(acac)_2$ complex, and this may account for the small differences observed in the EPR parameters. Additionally the spin density plots in Figure 3 show that the p orbital contribution to the singly occupied molecular orbital (SOMO) from the oxygen ligand atoms in the $Cu(acac)_2$ are not aligned with the Cu−O bond. This misalignment may have the effect of lowering the overall spin density around the Cu(II) metal center in the calculated values leading to a smaller $A_{||}$ value and larger $g_{||}$ value than observed experimentally.

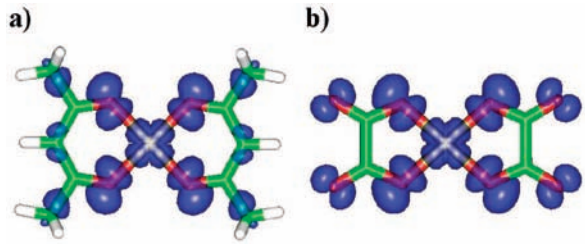

Figure 3. Spin density plots of (a) $Cu(acac)_2$ and (b) $[Cu(ox)_2]^{2-}$ complexes using the BP86 density functional gas phase calculations. The spin density plots calculated using the B3LYP functional are qualitatively similar. Plots generated using the gOpenMol software.[53,54]

The ability to reproduce the trend in $g_{||}$ and $A_{||}$ for the tetragonal copper complexes represents a significant advance in the application of DFT methods to copper model complexes. Furthermore, this suggests that DFT calculations can be used to calculate EPR parameters for related copper complexes and can provide additional structural insight, thus enhancing the interpretation of EPR experimental data.

Structural Insight and Calculated EPR Parameters. Peisach and Blumberg correlated the overall charge of a Cu(II) complex with the experimental $g_{||}$ and $A_{||}$ values for tetragonal Cu(II) complexes with similar equatorial ligands. This trend is reproduced quite well in the DFT calculations when comparing the Cu(II) aqua and hydroxy complexes, $[Cu(H_2O)_6]^{2+}$ and $[Cu(OH)_4]^{2-}$, which are at the extremes of the range for charges of the model complexes. The trend of increasing $g_{||}$ and decreasing $A_{||}$ with decreasing charge is not so clear when the $Cu(acac)_2$ and $[Cu(ox)_2]^{2-}$ complexes are included. $Cu(acac)_2$ is approximately where it should be based on the neutral charge, however, $[Cu(ox)_2]^{2-}$ should be closer to $[Cu(OH)_4]^{2-}$ in the upper lefthand corner of the graphs in Figure 2. It should be noted that the EPR parameters of the $Cu(acac)_2$ and $[Cu(ox)_2]^{2-}$ complexes are sensitive to the inclusion of axial ligands or counterions that change the geometry. For example, if a counterion is present in the coordination sphere of $[Cu(ox)_2]^{2-}$, then the charge changes from −2 to 0 for $Na_2[Cu(ox)_2]$. As shown in Tables 3 and 4 and discussed earlier, the $g_{||}$ and $A_{||}$ values systematically change when the axial ligands and/or counterions are present. Since the ligand environment for the experimental data for these two complexes is not entirely certain, the relative positions of these two complexes in Figure 2 remains inconclusive.

Close examination of the structural data generated by geometry optimization and the EPR parameters, both calculated with DFT methods, reveals that the trends in $g_{||}$ and $A_{||}$ for the copper complexes can be correlated with the equatorial Cu−O bond length. Figure 4a,b shows correlations between the average equatorial Cu−O bond lengths and the principle components of the **g**- and **A**-tensors, respectively. The graphs in Figure 4 show clear evidence that the position of the equatorial ligands has a significant impact on the EPR parameters. Figure 4 contains data obtained using the BP86 functional, but graphs generated using the B3LYP hybrid density functional data are qualitatively similar.

The Cu(II) complexes studied here all have a SOMO with a large amount of $d_{x^2-y^2}$ character. The interaction of the oxygen atoms of the equatorial ligands with the unpaired electron in the copper $d_{x^2-y^2}$ orbital provides a significant perturbation to the EPR parameters. The length of the Cu−O bond is qualitatively correlated to the amount of overlap between the copper and ligand atomic orbitals. Consequently the perturbation to the

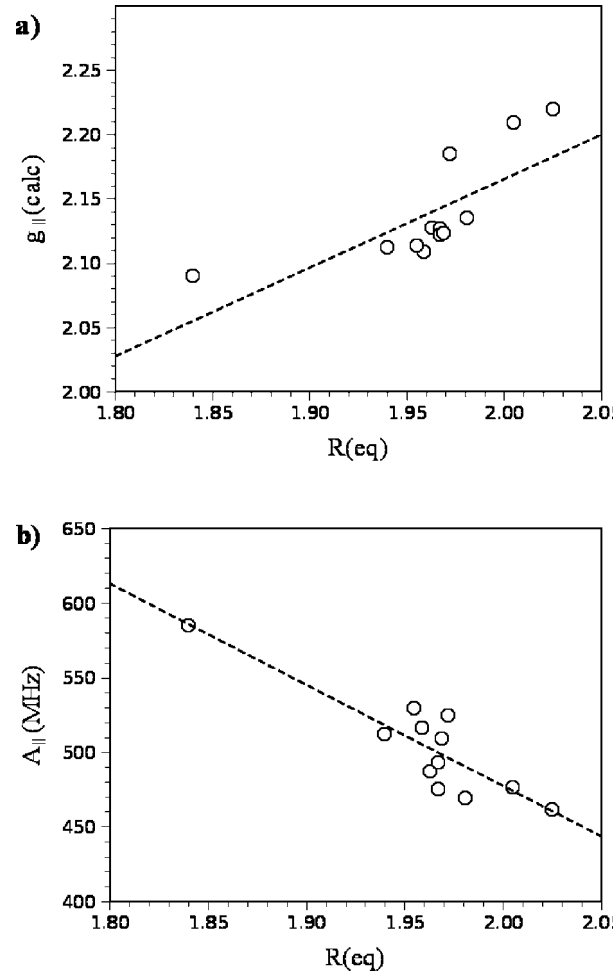

Figure 4. Correlations of average equatorial Cu−O bond lengths, R(eq), with EPR parameters calculated using the BP86 density functional for all complexes studied. Plots with EPR parameters calculated using the B3LYP hybrid density functional are qualitatively similar.

$d_{x^2-y^2}$ orbital on the copper atom depends principally on the Cu−O equatorial bond lengths. For molecules with relatively short Cu−O bond lengths the result is, in general, a smaller $g_{||}$ value and a larger $A_{||}$ value and the reverse is generally true for molecules with longer Cu−O bonds, as can be seen in Figure 4.

Interpretation of EPR Data for Copper-Exchanged Zeolites. To demonstrate how new insight can be provided through DFT calculations based on the reproduction of the observed trends in the EPR parameters, the copper complexes formed in copper-exchanged zeolites will be revisited. Previous experimental EPR studies of copper-exchanged zeolites were interpreted using the Peisach−Blumberg truth tables.[55,56] The analysis indicated that the copper complex in the hydrated zeolites, such as Cu-β, was most likely $[Cu(H_2O)_5OH]^+$ based on a comparison of the $g_{||}$ and $A_{||}$ for tetragonal copper model complexes with the experimental $g_{||}$ and $A_{||}$ for the Cu-zeolite complex ($g_{||}$ = 2.398, $A_{||}$ = 460 MHz). The EPR parameters for the copper complex in dehydrated Cu-β exhibited an increased $A_{||}$ (520 MHz) and a decreased $g_{||}$ ($g_{||}$ = 2.314) relative to the hydrated copper zeolite complexes. This was interpreted as a change in geometry and possibly ligation as the copper complex formed covalent bonds to the zeolite framework. These trends were observed in many different copper-exchanged zeolites suggesting that the copper complexes were structurally similar. Using

the DFT results presented here, the changes in $A_{||}$ and $g_{||}$ that are observed can be correlated with a decrease in the Cu−O equatorial bond length of approximately 0.05 and 0.15 Å for the hydrated and dehydrated copper-zeolite complexes, respectively, when compared to the fully hydrated Cu(II) complex, $[Cu(H_2O)_6]^{2+}$. Further work is in progress to use DFT methods to directly calculate the EPR parameters for copper-zeolite complexes. Previous results in the literature using the CASPT2 method (multiconfigurational perturbation theory) to calculate the EPR parameters for copper-zeolite complexes have demonstrated excellent agreement of calculated $g_{||}$ values with experimental $g_{||}$ values.[11] The CASPT2 results also show a trend of increasing Cu−O bond lengths with increasing $g_{||}$.

IV. Conclusions

Density functional theory was used to investigate the Cu(II) model complexes in the Peisach−Blumberg Cu(II) truth tables. Specifically the electron paramagnetic resonance parameters for complexes containing four oxygen atoms strongly coordinated to Cu(II) in a square planar arrangement were calculated using DFT calculations. The coordination of additional ligands to Cu(II) in axial positions giving the complex an overall square pyramidal or octahedral geometry was determined to have a significant impact on the optimized geometries and in turn the calculated EPR parameters for the complexes studied. For axially coordinating complexes the addition of axial ligands elongated the equatorial bond Cu−O bond lengths, localizing the electron density about Cu(II), in some cases resulting in significant shifts to the calculated EPR parameters.

The calculated EPR parameters ($g_{||}$ and $A_{||}$) for the complexes studied replicate the trends observed in the experimental plots constructed by Peisach and Blumberg. With increasing delocalization of charge about Cu(II), an increase in the calculated copper $A_{||}$ and decrease in the calculated $g_{||}$ was observed with either the GGA BP86 or hybrid B3LYP density functionals. Both functionals used in this study underestimate the $g_{||}$ values in a systematic manner, but the general trends are reproduced. For the model complexes, the calculated $A_{||}$ values are in good agreement with experimental $A_{||}$ values for DFT calculations with the BP86 functional, the exception being the $[Cu(H_2O)_6]^{2+}$ complex, for which the copper $A_{||}$ value is overestimated. With the B3LYP hybrid density functional, the copper $A_{||}$ value is systematically overestimated for the complexes studied here. The calculated results using the B3LYP functional provide the best replication of the experimentally observed $g_{||}$ and copper $A_{||}$ trend due to the systematic errors in the calculated values.

While current methodologies for calculating EPR parameters using DFT do not provide direct quantitative agreement with experimental results, a significant amount of insight into the structural characteristics of a complex can be obtained. The systematic nature of the errors inherent in calculating EPR parameters with DFT methods provides a suitable framework in which the trends in the EPR parameters can be replicated. Trends, such as the one presented here, provide experimental guidance for qualitative structural determinations. Similarly calculated trends can be used to validate structural assignments and models of interesting systems. The EPR parameter trend replicated with DFT shown here is an ideal tool to investigate the coordination environment of Cu(II) in proteins and in zeolites. A number of models for the geometry and position within the zeolite pores have been proposed using both experimental data and computational methods. Our results could be used as an invaluable tool to test the validity of proposed structures and coordination environments for hydrated and dehydrated Cu(II) exchanged zeolites.

Acknowledgment. W.M.A. acknowledges support from the University of Iowa Presidential graduate fellowship. Partial funding for this project was provided from the Center for Global and Regional Environmental Research at the University of Iowa.

Supporting Information Available: Calculated **g**-tensor and **A**-tensor values for each model complex. This material is available free of charge via the Internet at http://pubs.acs.org.

References and Notes

(1) Peisach, J.; Blumberg, W. E. *Arch. Biochem. Biophys.* **1974**, *165*, 691.
(2) Delabie, A.; Pierloot, K.; Groothaert, Marijke, H.; Schoonheydt, R. A.; Vanquickenborne, L. G. *Eur. J. Inorg. Chem.* **2002**, *2002*, 515.
(3) Bruschi, M.; Gioia, L. D.; Mitric, R.; Bonacic-Koutecky, V.; Fantucci, P. *Phys. Chem. Chem. Phys.* **2008**, *10*, 4573.
(4) Fritscher, J. *Phys. Chem. Chem. Phys.* **2004**, *6*, 4950.
(5) Goursot, A.; Berthomieu, D. *Magn. Reson. Chem.* **2004**, *42*, S180.
(6) Baute, D.; Arieli, D.; Neese, F.; Zimmermann, H.; Weckhuysen, B. M.; Goldfarb, D. *J. Am. Chem. Soc.* **2004**, *126*, 11733.
(7) Pezzato, M.; Lunga, G. D.; Baratto, M. C.; Sinicropi, A.; Pogni, R.; Basosi, R. *Magn. Reson. Chem.* **2007**, *45*, 846.
(8) Amini, S. K.; Hadipour, N. L.; Elmi, F. *Chem. Phys. Lett.* **2004**, *391*, 95.
(9) Benisvy, L.; Bittl, R.; Bothe, E.; Garner, C. D.; McMaster, J.; Ross, S.; Teutloff, C.; Neese, F. *Angew. Chem., Int. Ed.* **2005**, *44*, 5314.
(10) Pierloot, K.; Delabie, A.; Groothaert, M. H.; Schoonheydt, R. A. *Phys. Chem. Chem. Phys.* **2001**, *3*, 2174.
(11) Groothaert, M. H.; Pierloot, K.; Delabie, A.; Schoonheydt, R. A. *Phys. Chem. Chem. Phys.* **2003**, *5*, 2135.
(12) Delabie, A.; Pierloot, K.; Groothaert, M. H.; Weckhuysen, B. M.; Schoonheydt, R. A. *Phys. Chem. Chem. Phys.* **2002**, *4*, 134.
(13) Periyasamy, G.; Sundararajan, M.; Hillier, I. H.; Burton, N. A.; McDouall, J. J. W. *Phys. Chem. Chem. Phys.* **2007**, *9*, 2498.
(14) de Almeida, K. J.; Rinkevicius, Z.; Hugosson, H. W.; Ferreira, A. C.; Agren, H. *Chem. Phys.* **2007**, *332*, 176.
(15) Neese, F. Quantum Chemical Approaches to Spin-Hamiltonian Parameters. In *Electron Paramagnetic Resonance*; Gilbert, B. C., Davies, M. J., Murphy, D. M., Eds.; RCS Publications: Cambridge, 2007; Vol. 20, p 73.
(16) Munzarová, M. L. DFT Calculations of EPR Hyperfine Coupling Tensors In *Calculation of NMR and EPR Parameters*; Kaupp, M., Bühl, M., Malkin, V. G., Eds.; Wiley-VCH: Weinheim, 2004; p 463.
(17) Patchkovskii, S.; Schreckenbach, G. Calculations of EPR g-Tensors with Density Functional Theory In *Calculation of NMR and EPR Parameters*; Kaupp, M., Bühl, M., Malkin, V. G., Eds.; Wiley-VCH: Weinheim, 2004; p 505.
(18) Ban, F.; Gauld, J. W.; Boyd, R. J. Computation of Hyperfine Coupling Tensors to Compliment EPR Experiments In *Calculation of NMR and EPR Parameters*; Kaupp, M., Bühl, M., Malkin, V. G., Eds.; Wiley-VCH: Weinheim, 2004; p 567.
(19) Neese, F. Applications to EPR in Bioinorganic Chemistry. In *Calculation of NMR and EPR Parameters*; Kaupp, M., Bühl, M., Malkin, V. G., Eds.; Wiley-VCH: Weinheim, 2004; p 581.
(20) Torrent, M.; Musaev, D. G.; Morokuma, K.; Ke, S.-C.; Warncke, K. *J. Phys. Chem. B* **1999**, *103*, 8618.
(21) Asher, J. R.; Doltsinis, N. L.; Kaupp, M. *J. Am. Chem. Soc.* **2004**, *126*, 9854.
(22) Kim, S. H.; Aznar, C.; Brynda, M.; Silks, L. A.; Michalczyk, R.; Unkefer, C. J.; Woodruff, W. H.; Britt, R. D. *J. Am. Chem. Soc.* **2004**, *126*, 2328.
(23) Sinnecker, S.; Reijerse, E.; Neese, F.; Lubitz, W. *J. Am. Chem. Soc.* **2004**, *126*, 3280.
(24) Saladino, A. C.; Larsen, S. C. *J. Phys. Chem. A* **2003**, *107*, 1872.
(25) Neese, F. *J. Chem. Phys.* **2003**, *118*, 3939.
(26) Neese, F. *J. Chem. Phys.* **2001**, *115*, 11080.
(27) Neese, F. *J. Phys. Chem. A* **2001**, *105*, 4290.
(28) Malkina, O. L.; Vaara, J.; Schimmelpfennig, B.; Munzarova, M.; Malkin, V. G.; Kaupp, M. *J. Am. Chem. Soc.* **2000**, *122*, 9206.
(29) Kaupp, M.; Reviakine, R.; Malkina, O. L.; Arbuznikov, A.; Schimmelpfennig, B.; Malkin, V. G. *J. Comput. Chem.* **2002**, *23*, 794.
(30) Perdew, J. P.; Kurth, S.; Zupan, A.; Blaha, P. *Phys. Rev. Lett.* **1999**, *82*, 2544.
(31) Stefan, G. *J. Chem. Phys.* **2006**, *124*, 034108.
(32) Kossmann, S.; Kirchner, B.; Neese, F. *Mol. Phys.* **2007**, *105*, 2049.
(33) Neese, F. *J. Chem. Phys.* **2005**, *122*, 034107.
(34) Saladino, A. C.; Larsen, S. C. *J. Phys. Chem. A* **2003**, *107*, 5583.
(35) Neese, F. *ORCA - an ab initio, DFT and semiemperical program package*, 2.6.35 ed.; University of Bonn: Bonn, Germany, 2008.
(36) Becke, A. D. *Phys. Rev. A* **1988**, *38*, 3098.

(37) Lee, C.; Yang, W.; Parr, R. G. *Phys. Rev. B* **1988**, *37*, 785.
(38) Vosko, S. H.; Wilk, L.; Nusair, M. *Can. J. Phys* **1980**, *58*, 1200.
(39) Schafer, A.; Horn, H.; Ahlrichs, R. *J. Chem. Phys.* **1992**, *97*, 2571.
(40) Kendall, R. A.; Früchtl, H. A. *Theor. Chim. Acta* **1997**, *97*, 158.
(41) Neese, F. *J. Comput. Chem.* **2003**, *24*, 1740.
(42) Lebrun, P. C.; Lyon, W. D.; Kuska, H. A. *J. Chem. Crystallogr.* **1986**, *16*, 889.
(43) Gleizes, A.; Maury, F.; Galy, J. *Inorg. Chem.* **1980**, *19*, 2074.
(44) Perdew, J. P.; Wang, Y. *Phys. Rev. B* **1992**, *45*, 13244.
(45) Perdew, J. P. *Phys. Rev. B* **1986**, *33*, 8822.
(46) Neese, F. *Inorg. Chim. Acta* **2002**, *337*, 181.
(47) Ohtaki, H.; Radnai, T. *Chem. Rev.* **1993**, *93*, 1157.
(48) Persson, I.; Persson, P.; Sandstrom, M.; Ullstrom, A.-S. *J. Chem. Soc., Dalton Trans.* **2002**, 1256.
(49) Szilagyi, R. K.; Metz, M.; Solomon, E. I. *J. Phys. Chem. A* **2002**, *106*, 2994.
(50) Adato, I.; Eliezer, I. *J. Chem. Phys.* **1971**, *54*, 1472.
(51) Falk, K. E.; Ivanova, E.; Roos, B.; Vanngard, T. *Inorg. Chem.* **1970**, *9*, 556.
(52) Walker, F. A.; Sigel, H.; McCormick, D. B. *Inorg. Chem.* **1972**, *11*, 2756.
(53) Bergman, D. L.; Laaksonen, L.; Laaksonen, A. *J. Mol. Graphics Modell.* **1997**, *15*, 301.
(54) Laaksonen, L. *J. Mol. Graphics* **1992**, *10*, 33.
(55) Carl, P. J.; Larsen, S. C. *J. Phys. Chem. B* **2000**, *104*, 6568.
(56) Carl, P. J.; Larsen, S. C. *J. Catal.* **1999**, *182*, 208.
(57) Benfatto, M.; D'Angelo, P.; Della Longa, S.; Pavel, N. V. *Phys. Rev. B* **2002**, *65*, 174205.

JP810924J